The British Journal of Radiology, 78 (2005), 122–129 © 2005 The British Institute of Radiology
DOI: 10.1259/bjr/30866348

In vivo validation of a novel semi-automated method for border detection in intravascular ultrasound images

[1,3]C V BOURANTAS, MD, [2]M E PLISSITI, MSc, [2,3]D I FOTIADIS, PhD, [2]V C PROTOPAPPAS, MSc, [1,3]G V MPOZIOS, PhD, [1,3]C S KATSOURAS, MD, [2]I C KOURTIS, BSc, [4]M R REES, FRCP, FRCR and [1,3]L K MICHALIS, MD, MRCP

[1]*Department of Cardiology, Medical School,* [2]*Unit of Medical Technology and Intelligent Information Systems, Department of Computer Science, University of Ioannina,* [3]*Michailideion Cardiology Center, GR 45110 Ioannina, Greece and* [4]*University Department of Clinical Radiology, Bristol Royal Infirmary, Bristol BS2 8HW, UK*

Abstract. The aim of this work was to evaluate a new semi-automated intravascular ultrasound (IVUS) border detection method. The method was used to identify the lumen and the external elastic membrane or the borders of stents in 80 IVUS images, randomly selected from 10 consecutive human coronary arteries. These semi-automated results were compared with observations of two experts. Several indices in each case were obtained in order fully to evaluate the method. The time required for identification of the borders was also recorded. The interobserver variability of the method ranged from 1.21% to 5.61%, the correlation coefficient from 0.98 to 0.99, the slope was close to unity (0.94–1.03), the *y* intercept close to zero and the Williams index value was close to unity (range 0.67–0.91). The time (mean $\pm$ SD) required for the method to identify the borders of the different vessel layers for the whole IVUS sequence was 5.2 ± 0.2 min. The results demonstrate that the method is reliable and capable of identifying rapidly and accurately the different vessel layers depicted in IVUS images.

Intravascular ultrasound (IVUS) generates cross-sectional images of the coronary arteries with high temporal and spatial resolution. IVUS has been used for the evaluation of vessel wall morphology and dimensions [1–5] and has become an important method in many clinical and research applications [6–10].

IVUS cross-sectional images are generated by detecting the scattered waves of the ultrasound signal while this is passing through the vessel wall. A sequence of IVUS images is acquired during the withdrawal of an IVUS catheter through the artery. In each image, lumen, external elastic membrane, atheroma, calcium, stent and remodelling measurements can be performed [11].

The clinical applications of IVUS have been restricted because IVUS artefacts (*e.g.* non-uniform rotational distortion, guide wire shadow artefacts, ring-down effect and blood speckle artefacts) can reduce the ability to identify vessel wall layers and influence the accuracy of the obtained measurements. Manual border detection in IVUS images is laborious, time consuming and can be unreliable in the hands of an inexperienced operator [12]. To overcome these problems, automatic boundary detection methods have been reported. However these methods have not been able to resolve all issues related to reliability and speed [13–17]. In order to overcome some of the problems related to the usage of these previously reported automated methods we have developed a novel semi-automated method, which identifies accurately and quickly the different layers of the vessel wall [18].

The objective of this study was to evaluate this novel locally developed semi-automated method of IVUS border detection in a clinical setting.

Received 10 February 2004 and in revised form 26 June 2004, accepted 27 August 2004.

Materials and methods

Study group

The study group consisted of 10 consecutive patients (6 male, age range 52–72 years), who underwent IVUS examination for clinical purposes. The segments analysed were located in the left anterior descending artery (3), right coronary artery (5) and left circumflex coronary artery (2). Arterial segments with side branches were excluded for the purpose of this study, while segments with calcified plaques were included. In five out of the 10 coronary arteries assessed, stent implantation preceded the IVUS examination.

From each IVUS examination eight randomly selected IVUS images, spaced >1.5 mm apart from each other, were used for the validation of the method.

Intravascular ultrasound

The IVUS images were obtained using a 2.9 F, 30 MHz catheter (Avanar F/X, Endosonics, USA; catheter size 2.9 F, length 150 cm, maximum guide wire 0.014″, minimum guide catheter 5 F, tapered tip 0.022″). Sequential imaging was obtained with the IVUS catheter connected to a motorized pullback device operating at a speed of 0.5 mm s^{-1}. IVUS images were acquired at a standard rate of 10 frames s^{-1} and were digitized in a DICOM format. From each IVUS examination 60 s was digitized. The calibration markers, displayed on the digitized images, were used to derive the pixel size of 0.027 mm, which was used to calculate the cross-sectional areas and the perimeters of the different regions of interest.

Automated contour detection method

The lumen and external elastic membrane borders in each IVUS frame were extracted using the method

described by Plissiti et al [18]. The method is based on the principles of deformable models, and as a consequence, an initial estimation of the borders is required. However, the user's interaction is limited to only the first frame of the IVUS sequence, where an initial estimation for the lumen and the external elastic membrane borders must be provided. The method processes all frames automatically in a sequence using the borders detected in the previous frame as the initial parameters.

For each frame, initially a 3×3 median filter is applied to reduce artefacts and blood speckle. A linear filter is used for image enhancement. The initial estimation of the desired border constitutes the deformable model, which deforms finally to detect the border. In our model, the searching space is limited using perpendicular line segments to the initial contours, at even intervals. Predefined points of the line segments are candidate points for the desired border. The deformation of the model is based on the minimization of its energy function. The points corresponding to a global minimum of the energy function constitute the detected border.

The position of each point of the deformable model is given by the cartesian coordinates (x_i, y_i). The energy function, E_{snake}, is given as the sum of two terms,

$$\begin{aligned} E_{\text{snake}} &= \sum_{i=1}^{N} \left\{ E_{\text{int}}(x_i, y_i) + E_{\text{image}}(x_i, y_i) \right\} \\ &= \sum_{i=1}^{N} \left\{ a\left[(x_i - x_{i-1})^2 + (y_i - y_{i-1})^2\right] \right. \\ &\quad \left. + b\left[(x_{i-1} - 2x_i + x_{i+1})^2 + (y_{i-1} - 2y_i + y_{i+1})^2\right] - \gamma g_i \right\} \end{aligned}$$

where E_{int} represents the internal energy of the model due to bending and E_{image} is derived from image data. Factors a, b and γ are weights that regulate the contribution of each term and g_i is the image gradient of the (x_i, y_i) point. The energy function is minimized using a Hopfield neural network, combined with a simulated annealing schema [18]. The nodes of the network correspond to image pixels.

The convergence of the network might result in points that do not accurately describe the desired boundary, due to the complexity of IVUS images. To detect smooth edges that separate large regions of pixels having similar intensity, the gradient of the image at a specific pixel, which is incorporated in the image energy, is calculated using the mean intensity value of four adjacent square areas (windows) of fixed size. In this way, pixels with a large image gradient corresponding to noise speckle, which may have attracted the contour towards their position and entailed an incorrect identification of the borders, are excluded. We found that small distortions in the shape of the final contour may cause abnormalities in the specification of the searching area for the next frame. For this reason, we look for smooth initial estimations for the external elastic membrane border. From this the convex hull of the extracted border points is calculated, using the plane sweep approach [18].

In the images where calcified plaques exist, our method is capable of overcoming this problem using knowledge from previous frames [18]. The image segmentation method is applied twice on the entire sequence of IVUS frames. The first application results in the detection of the media/adventitia border and the second in the detection of the lumen border. The first border imposes the limitations in the searching space of the second border.

Validation of the proposed method

This new method was validated with regard to its ability to detect the borders of the lumen, the external elastic membrane and the stent against a gold standard. In order to produce the gold standard, two expert observers performed detection of the borders of the above layers in each IVUS frame twice with a month's interval between the two examinations. The mean estimation of the four total estimations was regarded as the gold standard. The mean estimation was extracted using an interpolation method [19].

The reproducibility of manual tracing was assessed by computing the interobserver and intraobserver variability for the area and perimeter of the regions of interest (lumen, external elastic membrane and stent).

Several ways were used to evaluate the performance of the method:

(a) The values of the areas and perimeters estimated by the automated border detection and those that had been detected by the two experts were compared (interobserver variability), correlated (linear regression analysis [20]) and finally their differences were estimated and compared (Williams index [21]).
(b) The surfaces of the regions of interest (lumen, external elastic membrane and stent) estimated by the automated border detection method were superimposed with the ones estimated using the interpolation method and the fit between the two corresponding surfaces was estimated (non-overlapping area analysis [17], Williams index for non-overlapping areas and Williams index for Hausdorff and mean distance).
(c) The time needed in order for the proposed method to detect the borders of the different layers in each IVUS sequence was reported.

Statistical analysis

The interobserver variability of the two observers for the values of area and perimeter was assessed by computing the mean and the standard deviation (SD) of the differences between the two observers' estimations. The intraobserver variability of each observer for the values of area and perimeter was estimated by computing the mean and the SD of the differences between the first and second tracing of each observer. The interobserver variability of our method was computed by assessing the mean and SD of the differences between our method and the mean estimation of the two observers.

For the linear regression analysis purposes, correlation coefficients, slope and y interception were computed.

The Williams index (WI) was calculated according to the following equation:

$$\text{WI} = \frac{\frac{1}{n}\sum_{j=1}^{n} \frac{1}{D_{0,j}}}{\frac{2}{n-1}\sum_{j}\sum_{j' \neq j} \frac{1}{D_{j,j'}}} \qquad (1)$$

where n is the number of observers, $D_{j,j'}$ is the average

difference between observers and $D_{0,j'}$ is the disagreement between our method and each observer. The Williams index confidence interval was estimated using a jack knife technique [21].

Williams index values close to unity imply that the difference between the results produced by an under evaluation method and the ones obtained by the observers is not larger than the difference between the observers. This suggests that the under evaluation method can be considered equally accurate with the expert observers. The non-overlapping area analysis in percentage was defined as the ratio of the non-overlapping areas (X regions in Figure 1) to the mean areas as they were extracted by the interpolation method. The intraobserver variability of each observer, the interobserver variability between the two observers and the interobserver variability of our method *vs* the expert observers were re-estimated using the non-overlapping area analysis.

The intraobserver variability (V_{intra}) was estimated by the equation [17]:

$$V_{\text{intra}} = \frac{1}{N} 100 \sum^{N} \frac{|A_1 - A_2|}{\frac{A_1 + A_2}{2}}, \quad (2)$$

where $A_1 - A_2$ represents the value of the non-overlapping areas, $\frac{A_1 + A_2}{2}$ is the area value of the mean estimation of an expert observer, and N is the number of IVUS images.

The interobserver variability (V_{inter}) between the two observers was estimated by the equation:

$$V_{\text{inter}} = \frac{1}{N} 100 \sum^{N} \frac{|A - B|}{\frac{A+B}{2}}, \quad (3)$$

where $A = \frac{A_1 + A_2}{2}$ and $B = \frac{B_1 + B_2}{2}$. A, B are the values of the mean estimation obtained from the first and second observer, respectively, using the interpolation method, $A - B$ represents the value of the non-overlapping areas between the mean estimations, $\frac{A+B}{2}$ is the value of the mean estimation of the two observers and N is the number of IVUS images.

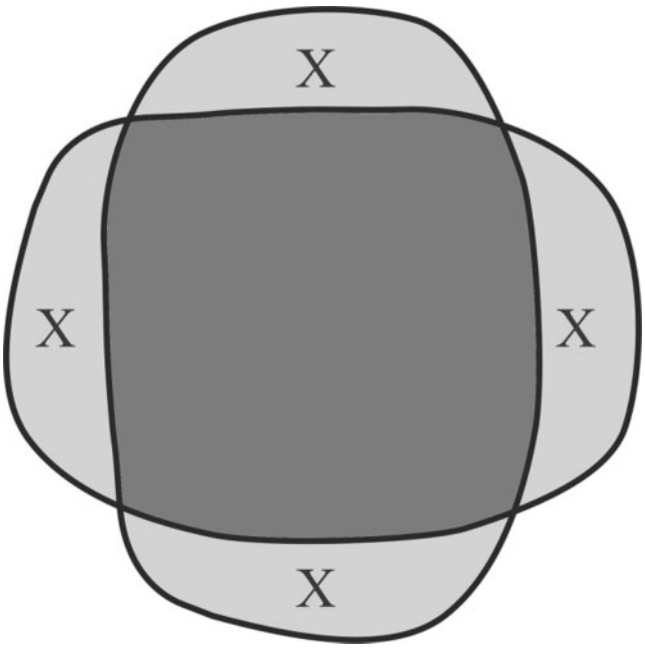

Figure 1. Two borders with the same area and perimeter value corresponding to geometrically different regions of interest. X indicates ratio of non-overlapping areas.

The interobserver variability ($V_{a\text{lg}}$) of our method was estimated by the equation:

$$V_{a\text{lg}} = \frac{1}{N} 100 \sum^{N} \frac{|C_{a\text{lg}} - (\frac{A+B}{2})|}{\frac{A+B}{2}}$$

where $|C_{a\text{lg}} - (\frac{A+B}{2})|$ represents the value of the non-overlapping areas between our method and the mean estimation of the two observers. The term $C_{a\text{lg}}$ is the estimation of our method.

The Hausdorff and mean distances were estimated after the definition of corresponding points in the borders, which had been detected by the observers and the automated method. In order for the corresponding points to be defined an ''object-based'' method was used [19]. The Hausdorff distance was defined as the maximum distance between the corresponding points of two contours and the mean distance as the average distance between the corresponding points of two contours. A Hausdorff distance value close to the mean distance implies similarity of the two detected contours, whereas a high difference value between these two distances implies dissimilarity (Figure 2).

Results

80 randomly selected frames were used for the validation of our method. 40 of the examined images were obtained from stented coronary artery segments. In these segments the experts, while being able to trace the stent, were not able to detect the external elastic membrane borders in 22 of the segments. In total, the method was evaluated for its ability to detect the borders of: (a) the lumen in 80 frames; (b) the external elastic membrane in 58 frames; and (c) the stent in 40 frames.

The interobserver and intraobserver variability of the two experts for the lumen, external elastic membrane and stent border based on the values of area and perimeter are shown in Tables 1 and 2, respectively.

The interobserver variability between our method and the two experts for the lumen area, the external elastic membrane and the stent is shown in Figures 3–5, respectively. Moreover the interobserver variability between the proposed method and the two observers was $-1.03\% \pm 2.26$ for the lumen perimeter, $0.04\% \pm 1.47$ for the external elastic membrane perimeter and -1.05 ± 1.63 for the stent perimeter.

The linear regression analyses between our method and the two expert observers for the lumen area, the external elastic membrane area and the stent area are illustrated in Figures 6–8, respectively. Moreover, for lumen perimeter, external elastic membrane perimeter and the stent perimeter the linear regression analysis produced slopes of 1.03, 0.97 and 0.94, respectively, with y intercepts of -0.22 mm, 0.47 mm, and 0.43 mm. The correlation coefficients, between our method and the two observers, for the lumen perimeter, the external elastic membrane perimeter and the stent perimeter were 0.99, 0.99 and 0.98, respectively.

The Williams index for area and perimeter values is shown in Table 3.

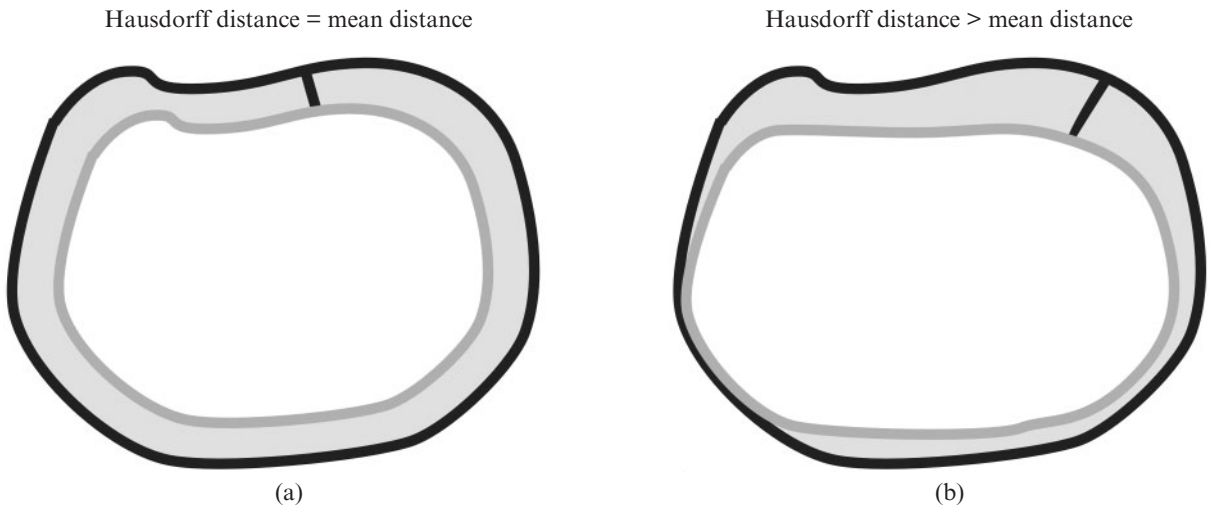

Figure 2. In figures (a) and (b) the non-overlapping areas are the same. The similarity in two border estimations is higher in figure (a) where the Hausdorff and the mean distance have the same value than in figure (b) where Hausdorff is larger than mean distance.

Table 1. Lumen, external elastic membrane and stent area variability. Results are presented as mean ± standard deviation

Variability	Lumen $N=80$	External elastic membrane $N=58$	Stent $N=40$
Intraobserver (1) variability (%)	1.92 ± 4.77	0.34 ± 2.65	0.16 ± 3.57
Intraobserver (2) variability (%)	0.60 ± 3.84	0.15 ± 1.87	0.87 ± 3.64
Interobserver variability (%)	0.97 ± 4.38	0.85 ± 2.07	1.10 ± 2.94

The non-overlapping area analysis is outlined in Table 4. The interobserver variability between our method and the two observers for the non-overlapping areas for the lumen, external elastic membrane and stent is illustrated in Figures 9–11, respectively. The Williams index for non-overlapping areas is given in Table 5. Finally the Williams index for Hausdorff and mean distances are shown in Table 6. The computer time required for the extraction of the regions of interest in a sequence of 600 IVUS images was 5.2 ± 0.2 min using a Pentium 4 computer with a 1.2 GHz processor and a 256 KB RAM memory.

Table 2. Lumen, external elastic membrane and stent perimeter variability. Results are presented as mean ± standard deviation

Variability	Lumen $N=80$	External elastic membrane $N=58$	Stent $N=40$
Intraobserver (1) variability (%)	0.89 ± 2.74	0.37 ± 1.67	0.2 ± 2.36
Intraobserver (2) variability (%)	0.57 ± 2.31	0.02 ± 1.40	0.62 ± 2.19
Interobserver variability (%)	0.54 ± 2.57	0.47 ± 0.71	0.51 ± 1.52

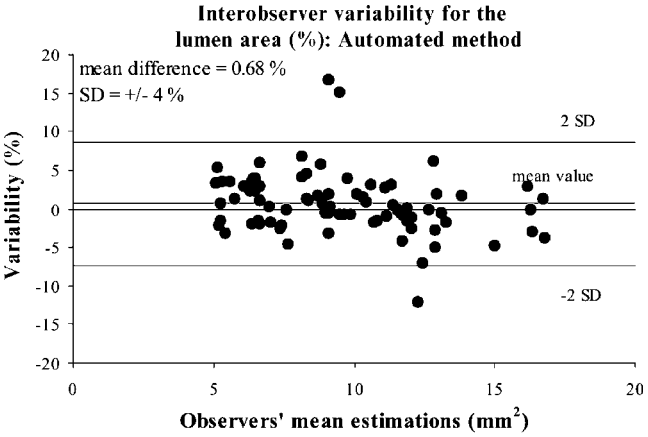

Figure 3. The interobserver variability between the contour detection method and the two observers for the lumen area. SD, standard deviation.

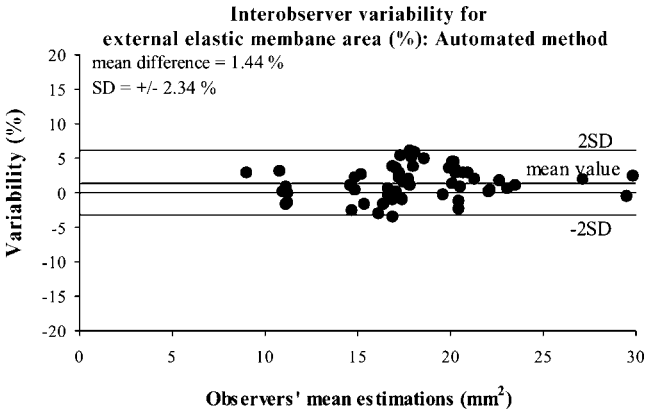

Figure 4. The interobserver variability between the contour detection method and the two observers for the external elastic membrane area. SD, standard deviation.

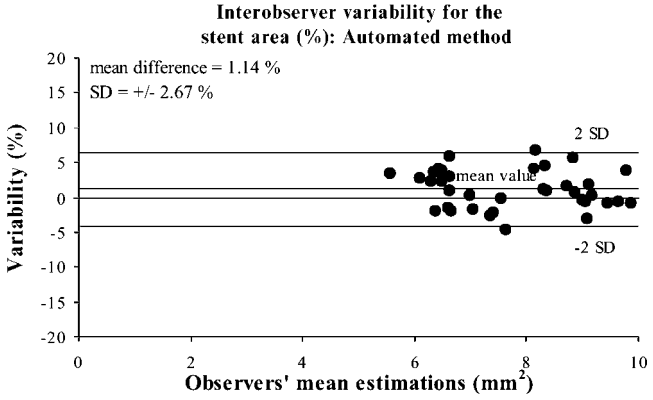

Figure 5. The interobserver variability between the contour detection method and the two observers for the stent area. SD, standard deviation.

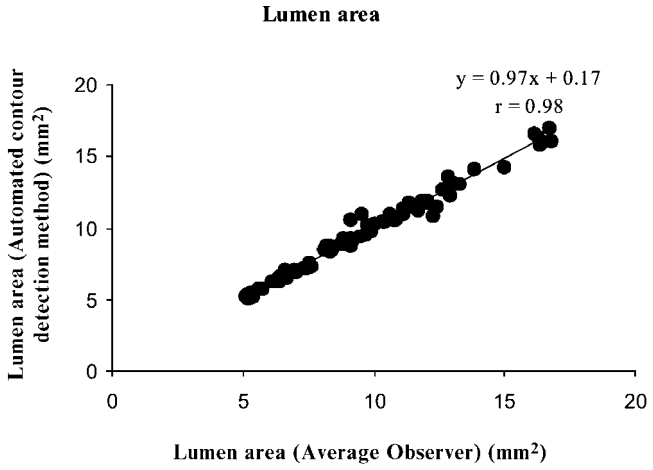

Figure 6. Linear regression analysis of the automatic lumen area *vs* manual tracing.

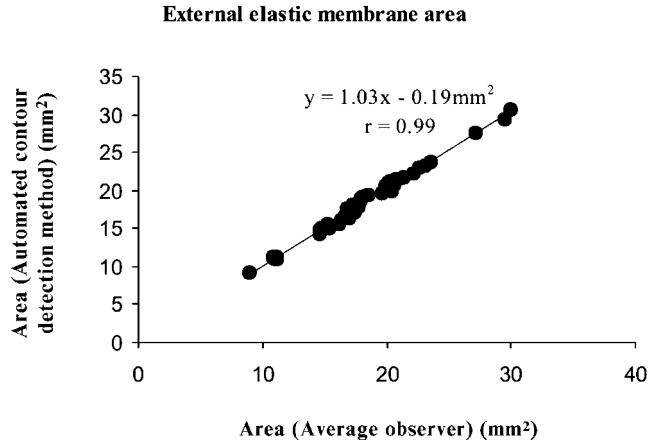

Figure 7. Linear regression analysis for the external elastic membrane area between the automatic and manual tracing.

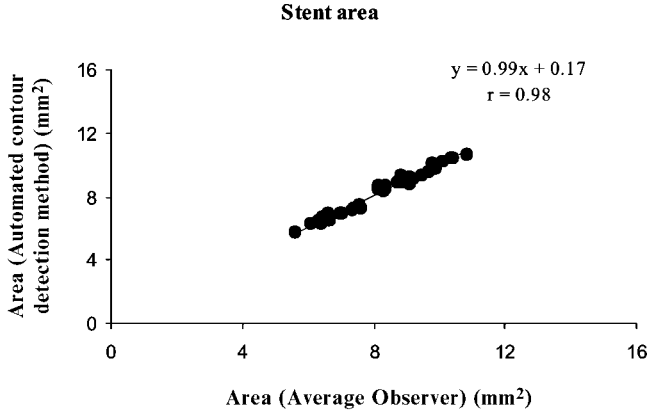

Figure 8. Linear regression analysis of the automatic stent area *vs* manual tracing.

Table 3. Williams index (WI) and 95% confidence intervals (CI) for areas and perimeters

	WI	CI (95%)
Lumen (area)	0.91	(0.89, 0.93)
Lumen (perimeter)	0.84	(0.82, 0.86)
External elastic membrane (area)	0.67	(0.64, 0.70)
External elastic membrane (perimeter)	0.81	(0.78, 0.84)
Stent (area)	0.82	(0.78, 0.86)
Stent (perimeter)	0.73	(0.69, 0.77)

Table 4. Interobserver and intraobserver variability for non-overlapping areas. Results are presented as mean ± standard deviation

Variability	Lumen $N=80$	External elastic membrane $N=58$	Stent $N=40$
Intraobserver (1) variability (%)	6.64 ± 3.88	3.88 ± 1.38	5.16 ± 2.16
Intraobserver (2) variability (%)	5.95 ± 2.47	3.62 ± 0.92	5.58 ± 2.12
Interobserver variability (%)	5.40 ± 2.86	3.29 ± 1.39	4.23 ± 1.36
Interobserver variability (automated method)	5.61 ± 2.79	3.75 ± 1.05	4.99 ± 1.39

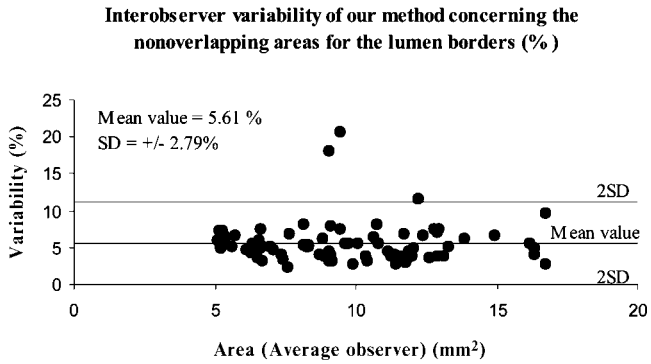

Figure 9. The interobserver variability between our method and the two observers concerning the non-overlapping areas for the lumen borders. SD, standard deviation.

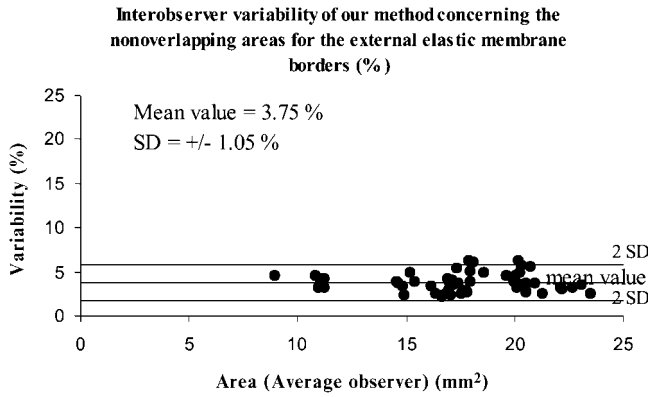

Figure 10. The interobserver variability between our method and the two observers concerning the non-overlapping areas for the external elastic membrane borders. SD, standard deviation.

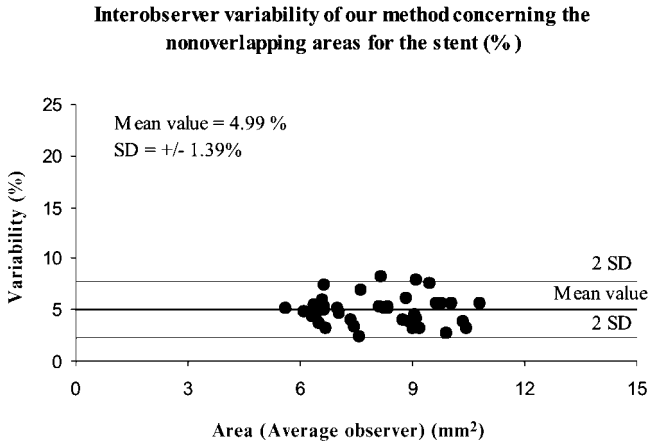

Figure 11. The interobserver variability between our method and the two observers concerning the non-overlapping areas for the stent borders. SD, standard deviation.

Table 5. Williams index (WI) and 95% confidence intervals (CI) for the non-overlapping areas

	WI	CI (95%)
Lumen	0.91	(0.90, 0.92)
External elastic membrane	0.79	(0.77, 0.81)
Stent	0.82	(0.81, 0.83)

Table 6. Williams index (WI) and 95% confidence interval (CI) for Hausdorff distance and mean distance

	WI	CI (95%)
Lumen (Hausdorff distance)	0.88	(0.87, 0.89)
External elastic membrane (Hausdorff distance)	0.88	(0.87, 0.89)
Stent (Hausdorff distance)	0.90	(0.88, 0.92)
Lumen (Mean distance)	0.90	(0.89, 0.91)
External elastic membrane (Mean distance)	0.89	(0.88, 0.90)
Stent (Mean distance)	0.82	(0.81, 0.83)

Discussion

IVUS depicts cross-sectional images of coronary arteries which provide accurate information of coronary artery morphology. Processing of such images by manual segmentation of IVUS has restricted its clinical applicability because manual processing is a tedious, difficult to reproduce and time-consuming procedure and requires considerable expertise. There has been considerable research effort to develop accurate automated methods for the detection of tissue and stent borders in IVUS images. These methods have several limitations due to the lack of homogeneity of tissue, and the high intensity variation that occurs in sampled regions of interest in IVUS images.

In an attempt to increase the clinical applicability of IVUS we have developed a novel semi-automated contour detection method. This method is based on the basic principles of deformable models and involves the incorporation of *a priori* knowledge, provided by an expert observer. The use of a Hopfield neural network makes the application of our method in individual frames fast and efficient. The method addresses common problems in IVUS segmentation such as the computation of the external elastic membrane in images where calcified lesions are present. In addition, our method overcomes the blood speckle artefacts and the guide wire shadow artefact, which have been previously described [18].

Several indices have been used for the validation of the fully automated method (*e.g.* automated method interobserver variability, Williams Index for area and perimeter, Hausdorff and mean distance to the detected borders). This has been achieved by applying direct comparison, linear regression analysis and non-overlapping area analysis. Our results indicate that the accuracy and the reliability of our method is high.

The reliability of the two observers is assessed using interobserver and intraobserver variability. Interobserver variability for area ranges from 0.85% to 1.1%, for perimeter from 0.47% to 0.54% and for non-overlapping areas from 3.29% to 5.4%. The above values confirm the accuracy and the reproducibility of the two observers and compare well with others reported in the literature [12]. The results demonstrate that the variability of the two observers is higher for the lumen borders. The difficulty in detecting the lumen border is probably caused by the speckle artefacts and by the irregularities of the lumen shape.

Linear regression analysis results indicate that the method is accurate. The slopes are close to unity, the y intercept always close to zero and the correlation coefficient is higher than 0.98 in all cases. The worst performance according to linear regression is obtained for the perimeter of the stent. This is due to the fact that the segmentation algorithm placed the stent borders at the pixels with the maximum image gradient and not at the stent struts as the observers did (Figure 12).

For non-overlapping areas, the Williams index ranges from 0.79 to 0.91. The obtained Williams index for the lumen is higher than the Williams index for the stent, although the interobserver variability (between the method and the mean manual estimation) exhibits a lower value for the stent. This discrepancy can be attributed to the low interobserver variability (between experts) for the stent, which decreases the value of the Williams index.

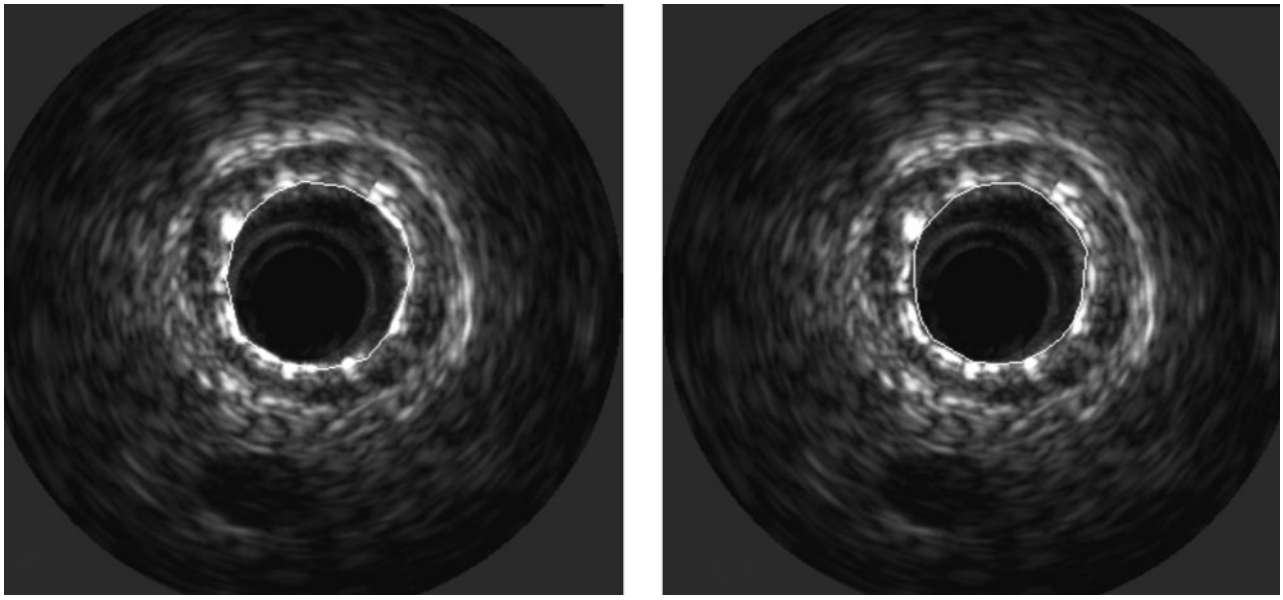

(a) (b)

Figure 12. Stent border detection in an intravascular ultrasound frame by (a) an expert observer and by (b) our automated segmentation method.

The influence of the interobserver variability (between the experts), according to the non-overlapping areas, on the Williams index can be also demonstrated in the external elastic membrane border. In this case the relatively low value of the Williams index (0.79) stems from the high agreement between the two observers and not from the poor performance of our method. The above remarks show that the interobserver variability must be taken into account, when discussing values of the Williams index.

Finally, the Williams indices for the Hausdorff distance and values for mean distance are close to unity (range from 0.88 to 0.90 and from 0.82 to 0.90, respectively). The above results demonstrate that the borders detected by our method have similar shape to those detected by the expert observers.

The task of identifying the regions of interest in IVUS images is a challenging one. Several algorithms have been developed in order to trace automatically the lumen and external elastic membrane borders and several methodologies have been used in order to assess their reliability [12, 14–17, 22–24]. Our method has certain advantages. By exploiting the similarity of sequential frames, user interaction is required only in the first frame of a sequence. The modification of the energy function of the deformable model makes the use of a Hopfield neural network feasible for the minimization of the energy function, which results in the reduction of the processing time for each frame. The introduction of a new expression for the image energy makes the method robust, resulting in accurate boundaries for all images. Our validation methodology is a systematic quantitative validation which employs additional quantitative metrics in addition to the metrics introduced by other researchers [12, 14–15, 17, 23–24]. These quantitative metrics describe further characteristics of the algorithm such as the shape similarity between the borders detected by our method and those detected by the expert observers.

However, our method has certain limitations. First, some tuning of the parameters must be carried out, in order to obtain acceptable values for the weight factors of our deformable model's energy function. In addition, the proposed method cannot accurately extract the region of interest in IVUS images where side branches exist. The energy function is re-instated without manual intervention in the following IVUS images, where no side branches exist.

In conclusion, this new semi-automated method for border detection in IVUS images is able to determine efficiently and quickly the lumen, external elastic membrane and stent borders, overcoming previously reported difficulties and thus extending the clinical applicability of IVUS imaging.

References

1. Nishimura RA, Edwards WD, Warnes CA, Reeder GS, Holmes DR, Tajik AJ, et al. Intravascular ultrasound imaging: in vitro validation and pathologic correlation. J Am Coll Cardiol 1990;16:145–54.
2. Potkin BN, Bartorelli AL, Gessert JM, Neville RF, Almagor Y, Roberts WC, et al. Coronary artery imaging with intravascular high-frequency ultrasound. Circulation 1990;81:1575–85.
3. Mallery JA, Tobis JM, Griffith J, Gessert J, McRay M, Moussabeck O, et al. Assessment of normal and atherosclerotic arterial wall thickness with an intravascular ultrasound imaging catheter. Am Heart J 1990;119:1392–400.
4. Nissen SE, Gurley JC, Grines CL, Booth DC, McClure R, Berk M, et al. Intravascular ultrasound assessment of lumen size and wall morphology in normal subjects and patients with coronary artery disease. Circulation 1991;84:1087–99.
5. De Feyter PJ, Serruys PW, Davies MJ, Richardson P, Lubsen J, Oliver MF. Quantitative coronary angiography to measure progression and regression of coronary atherosclerosis. Value, limitations, and implications for clinical trials. Circulation 1991;84:412–23.
6. Von Birgelen C, Airiian SG, Mintz GS, van der Giessen WJ, Foley DP, Roelandt JR, et al. Variations of remodeling in response to left main atherosclerosis assessed with intravascular ultrasound in vivo. Am J Cardiol 1997;80:1408–13.

7. Lansky AJ, Mintz GS, Popma JJ, Pichard AD, Kent KM, Satler LF, et al. Remodeling after directional coronary atherectomy (with and without adjunct percutaneous transluminal coronary angioplasty): a serial angiographic and intravascular ultrasound analysis from the optimal atherectomy restenosis study. J Am Coll Cardiol 1998;32:329–37.
8. Mehran R, Dangas G, Mintz GS, Lansky AJ, Pichard AD, Satler LF, et al. Atherosclerotic plaque burden and CK-MB enzyme elevation after coronary interventions: intravascular ultrasound study in 2256 patients. Circulation 2000;101:604–10.
9. Von Birgelen C, Mintz GS, Eggebrecht H, Herrmann J, Matthias J, Brinkoff J, et al. Preintervention arterial remodeling affects vessel stretch and plaque extrusion during coronary stent deployment as demonstrated by three dimensional intravascular ultrasound. Am J Cardiol 2003;92:130–5.
10. Nissen SE, Tsunoda T, Tuzcu EM, Schoenhagen P, Cooper CJ, Yasin M, et al. Effect of recombinant ApoA-I Milano on coronary atherosclerosis in patients with acute coronary syndromes: a randomized controlled trial. JAMA 2003;290:2292–300.
11. Mintz GS, Nissen SE, Anderson WD, Bailey SR, Elber R, Fitzgerald PJ, et al. American College of Cardiology clinical expert consensus document on standards for acquisition, measurement and reporting of intravascular ultrasound studies: a report of the American College of Cardiology task force on clinical expert consensus documents (committee to develop a clinical expert consensus on standards for acquisition, measurement and reporting of intravascular ultrasound studies [IVUS]). J Am Coll Cardiol 2001;37:1478–92.
12. Meier DS, Cothren RM, Vince DG, Cornhill JF. Automated morphometry of coronary arteries with digital image analysis of intravascular ultrasound. Am Heart J 1997;133:681–90.
13. Li W, von Birgelen C, Di Mario C, Boersma E, Gussenhoven E, var der Putten N, et al. Semi automatic contour detection for volumetric quantification of intracoronary ultrasound. In: Computers in Cardiology 1994. Los Alamitos, CA: IEEE Computer Society Press, 1994:277–280.
14. Mojsilovic A, Popovic M, Amodaj N, Babic R, Ostojic M. Automatic segmentation of intravascular ultrasound images: a texture-based approach. Ann Biomed Eng 1997;25:1059–71.
15. Zhang X, McKay C, Sonka M. Tissue catheterization in intravascular ultasound images. IEEE Trans Med Imaging 1998;17:889–99.
16. Shekhar R, Cothern RM, Vince DG, Chandra S, Thomas JD, Cornhill JF. Three-dimensional segmentation of luminal and adventitial borders in serial intravascular ultrasound images. Comput Med Imaging Graphics 1999;23:299–309.
17. Kovalski G, Beyear R, Shofti R, Azhari H. Three-dimensional automatic quantitative analysis of intravascular ultrasound images. Ultrasound Med Biol 2000;26:527–37.
18. Plissiti ME, Fotiadis DI, Michalis LK, Mpozios GM. An automated method for lumen and media/adventitia borders detection in a sequence of IVUS frames. IEEE Trans Inf Technol Biomed 2004;8:131–41.
19. Goshtasby A, Turner DA, Ackermann LV. Matching of tomographic slices for interpolation. IEEE Trans Med Imaging 1992;11:507–16.
20. Bland JM, Altman DG. Statistical methods for assessing agreement between two methods of clinical measurement. The Lancet 1986;1:307–10.
21. Chalana V, Kim Y. A methology for evaluation of boundary detection algorithm on medical images. IEEE Trans Med Imaging 1997;16:642–52.
22. Klingensmith JD, Sheknar R, Vince DG. Evaluation of three-dimensional segmentation algorithms for the identification of luminal and medial-adventitial borders in intravascular ultrasound images. IEEE Trans Med Imaging 2000;19:996–1011.
23. Von Birgelen C, Di Mario C, Li W, Schuurbiers CH, Slager CJ, de Feyter PJ, et al. Morphometric analysis in tree-dimensional intracoronary ultrasound: an in vitro and in vivo study performed with a novel system for the contour detection of lumen and plaque. Am Heart J 1996;132:516–27.
24. Koning G, Dijkstra J, Von Birgelen C, Tuinenburg JC, Brunette J, Tardif JC, et al. Advanced contour detection for three-dimensional intracoronary ultrasound: a validation in vitro and in vivo. Int J Cardiovasc Imag 2002;18:235–48.